Impact of experimentally measured relative permeability hysteresis on reservoir-scale performance of underground hydrogen storage (UHS)

Bo, Zhenkai ; Boon, Maartje ; Hajibeygi, Hadi ; Hurter, Suzanne

DOI
10.1016/j.ijhydene.2022.12.270

Publication date
2023

Document Version
Final published version

Published in
International Journal of Hydrogen Energy

Available online at www.sciencedirect.com

ScienceDirect

journal homepage: www.elsevier.com/locate/he

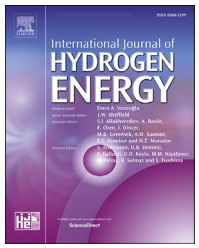

Impact of experimentally measured relative permeability hysteresis on reservoir-scale performance of underground hydrogen storage (UHS)

Zhenkai Bo [a,b,*], *Maartje Boon* [b], *Hadi Hajibeygi* [b], *Suzanne Hurter* [a,c]

[a] *Centre for Natural Gas, University of Queensland, St Lucia, Brisbane, 4072, Queensland, Australia*
[b] *Faculty of Civil Engineering and Geosciences, Delft University of Technology, P.O. Box 5048, Delft, 2600 GA, the Netherlands*
[c] *TNO, Applied Geosciences, Princetonlaan 6, Utrecht, the Netherlands*

HIGHLIGHTS

- Experimentally measured hydrogen-brine relative permeability curves show distinct characteristics compared to that of other fluid systems.
- UHS performances under different relative permeability curves are compared.
- Relative permeability curves from other fluid systems are not suitable to act as proxy to hydrogen-brine system in reservoir-scale UHS simulation.

ARTICLE INFO

Article history:
Received 17 October 2022
Received in revised form
21 December 2022
Accepted 22 December 2022
Available online 9 January 2023

Keywords:
Underground hydrogen storage
Relative permeability hysteresis
Reservoir simulation

ABSTRACT

Underground Hydrogen Storage (UHS) is an emerging large-scale energy storage technology. Researchers are investigating its feasibility and performance, including its injectivity, productivity, and storage capacity through numerical simulations. However, several ad-hoc relative permeability and capillary pressure functions have been used in the literature, with no direct link to the underlying physics of the hydrogen storage and production process. Recent relative permeability measurements for the hydrogen-brine system show very low hydrogen relative permeability and strong liquid phase hysteresis, very different to what has been observed for other fluid systems for the same rock type. This raises the concern as to what extend the existing studies in the literature are able to reliably quantify the feasibility of the potential storage projects. In this study, we investigate how experimentally measured hydrogen-brine relative permeability hysteresis affects the performance of UHS projects through numerical reservoir simulations. Relative permeability data measured during a hydrogen-water core-flooding experiment within ADMIRE project is used to design a relative permeability hysteresis model. Next, numerical simulation for a UHS project in a generic braided-fluvial water-gas reservoir is performed using this hysteresis model. A performance assessment is carried out for several UHS scenarios with different drainage relative permeability curves, hysteresis model coefficients, and injection/production rates. Our results show that both gas and liquid relative permeability hysteresis play an important role in UHS irrespective of injection/production rate. Ignoring gas hysteresis may cause up to 338% of uncertainty on cumulative hydrogen production, as

* *Corresponding author*. Centre for Natural Gas, University of Queensland, St Lucia, Brisbane, 4072, Queensland, Australia.
E-mail address: z.bo@uq.net.au (Z. Bo).

https://doi.org/10.1016/j.ijhydene.2022.12.270

it has negative effects on injectivity and productivity due to the resulting limited variation range of gas saturation and pressure during cyclic operations. In contrast, hysteresis in the liquid phase relative permeability resolves this issue to some extent by improving the displacement of the liquid phase. Finally, implementing relative permeability curves from other fluid systems during UHS performance assessment will cause uncertainty in terms of gas saturation and up to 141% underestimation on cumulative hydrogen production. These observations illustrate the importance of using relative permeability curves characteristic of hydrogen-brine system for assessing the UHS performances.

Introduction

Consensus has been reached worldwide that net zero carbon dioxide emissions should be achieved by 2050 to keep the global temperature rise below 2 °C above pre-industrial levels [1]. Hence, the transition from fossil fuels to low-carbon energy sources is crucial. This has led to an increase in research interest in renewable energy production as well as storage related technologies [2–5], that can resolve the intermittency problem that accompanies renewable energy generation [6]. For the coupling of energy storage to energy production and demand at the scale of GW, and a discharge time at a scale of months, Underground Gas Storage (UGS), Underground Hydrogen Storage (UHS), and pumped hydro power are the main feasible known technologies [7,8]. Pumped hydro power and UGS are already mature technologies with decades of operational experiences [9,10]. As a result, UHS is an emerging large-scale energy storage technology, embedded within the emerging hydrogen economy, which is at the centre of many research activities in recent years [11–14].

Underground hydrogen storage refers to the storage of energy in the form of hydrogen in subsurface reservoir units, which can be salt caverns, saline aquifers, and depleted oil and gas reservoirs. The storage takes place during periods in which energy production exceeds energy demand. The stored hydrogen will be reclaimed back to the surface when the demand is more than the production [11]. While hydrogen can be stored at a high degree of purity in salt caverns, because of the limited risk of contamination, their limited scale and availability makes them insufficient to satisfy the entire storage demand. Therefore, porous reservoirs are also considered since they are geographically abundant and can provide the volumetric capacity needed for larger scale UHS, albeit probably with a lower degree of purity.

To assess the feasibility of UHS in porous reservoirs, numerical simulations can be performed to study their injectivity, productivity, and storage capacity [10,13]. In addition, site selection and ranking criteria are also important research objectives of reservoir simulation studies, where reservoir structure and dip angle have been proposed to be key parameters for the productivity of UHS [15]. A common simulation schedule would be to start from initial injection of cushion gas progressing to several injection/production cycles of hydrogen [16–18], or prolonged production to evaluate ultimate hydrogen recovery [19,20]. In this study, hydrogen recovery refers to the ratio between total produced hydrogen and total injected hydrogen (including cushion gas) after cyclic operations.

Recent reservoir simulation studies have shown very low cyclic hydrogen recovery ranging from 14% in gas reservoirs [20], to 31% in saline aquifers [17], and to 43% in condensate gas reservoirs [19]. Furthermore, unless huge amounts of cushion gas were injected [20], considerable amounts of water or alternative cushion gas were being produced together with the hydrogen [17,19]. These simulation efforts, however, did not capture the flow and transport characteristics of the hydrogen/cushion gas/brine system accurately. Given the potential key role underground hydrogen storage could play for the energy transition [21–24], efforts should be put into more accurate simulations of hydrogen/cushion-gas/brine multi-phase flow in subsurface porous reservoirs, to reliably determine its feasibility.

During the cyclic storage of hydrogen in porous reservoirs, brine will displace the stored hydrogen gas towards the production well during the production period, where, at the fringe of this shrinking gas cap, imbibition will happen. In a water-wet sandstone reservoir [25,26], residual trapping will cause the hydrogen phase to be cut at the pore throat and isolated within the pore space (snap-off) as liquid saturation increases [27,28]. Also larger scale capillary heterogeneity trapping [29] will immobilize hydrogen and alter the relative permeability of the gas and the liquid phases such that they will be different from that of the primary drainage process. This path-dependent irreversibility of relative permeability behavior is called hysteresis, which has been extensively studied for oil-water-gas three-phase flow [30–32], and carbon dioxide geo-sequestration [33–35]. For the hydrogen-brine system, hysteresis has also been proven to exist through experiments [36,37]. The recently experimentally measured hydrogen-brine relative permeability data (including imbibition) show very different characteristics to that of other fluid systems. Specifically, after decades of experimental investigation in the oil-water-gas system, it is generally concluded that the most wetting phase shows minor hysteresis (e.g., Alizadeh and Piri, 2014) [31]. A similar conclusion is also made through many studies for the carbon dioxide-brine system (e.g., Juanes et al., 2006) [34]. Based on the currently available experimental observations, this is different for the hydrogen-brine system. For example, compared with experimental data for the carbon dioxide-brine and oil-water-gas systems, shown in Fig. 1a, the hydrogen relative permeability during imbibition (dotted line) is extremely low. Also, in contrast to the weak hysteresis in the wetting phase for other fluid systems, the liquid phase relative permeability hysteresis for the hydrogen-brine

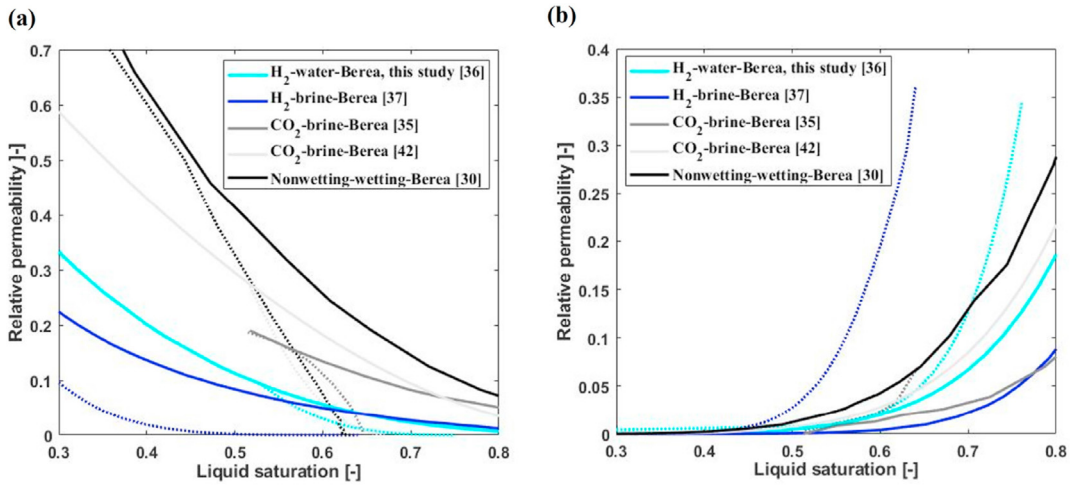

Fig. 1 – (a) Comparison of experimentally measured drainage (solid lines) and imbibition (dotted lines) gas phase relative permeability curves in Berea sandstone core samples for: H_2-water/brine (Boon et al., 2022 [36], Lysyy et al., 2022 [37]), CO_2-brine (Akbarabadi et al., 2013 [35], Krevor et al., 2012 [42]) and Oil-water-gas (Oak [30]); (b) experimentally measured drainage and imbibition liquid phase relative permeability curves for the same studies as listed under (a).

system is much stronger. Similar observations can also be made when comparing with relative permeability curves measured for other rock types from the oil and gas industry [17,32,38]. However, from Table 1, one can find that currently most UHS reservoir-scale simulation studies ignore realistic multi-phase flow behavior because few of them consider hysteresis [39,40]. Furthermore, arbitrary relative permeability models such as Brooks-Corey (BC) [16] and Van Genuchten (VG) [17,39], are being used or relative permeability data measured for fluid-rock systems other than hydrogen-brine-rock system [20,40,41]. Whether the results obtained from these simulation studies accurately represent the behavior of hydrogen is still in doubt. To our knowledge, the effects of using actual hydrogen relative permeability hysteresis data has not yet been studied.

In this study, the importance of experimentally measured hydrogen relative permeability hysteresis for the estimation of hydrogen recovery, water production, and the gas saturation distribution is investigated which are three feasibility indicators in UHS reservoir simulation studies that are intensely debated [17–19]. For this purpose, hydrogen-water relative permeability data, including for the imbibition process, measured during core-flooding experiments are used to build a relative permeability hysteresis model [36]. Next, this hysteresis model is incorporated into a commercial compositional reservoir simulator to perform numerical simulation for a generic braided-fluvial water-gas reservoir to systematically study the effects of relative permeability hysteresis (including both gas and liquid phase hysteresis) on the assessment of UHS projects. Finally, simulation results using hydrogen relative permeability curves are compared with simulation results when carbon dioxide (as a proxy of other fluid systems) relative permeability curves are used to further illustrate the importance of using relative permeability curves (including imbibition) with characteristic of the hydrogen-brine system for assessing UHS performance.

The structure of this paper is as follows: in Section 2 Methodology, first the experiment from which the relative permeability hysteresis data is taken for this study is described, and then the models chosen for the relative permeability hysteresis are discussed. Moreover, the reservoir simulation set up for assessing the effects of hysteresis is also described in Section Methodology. Section Results and discussion presents the results of our reservoir simulations and related discussions. Finally, the main conclusions are summarized in Section Conclusion.

Methodology

Core-flooding experiment and core sample properties

The relative permeability, for both drainage and imbibition, and capillary pressure are taken from a very recent hydrogen-

Table 1 – Overview of relative permeability models in recent UHS simulation studies.

Reference	Relative permeability model	Hysteresis
Feldmann F. et al., 2016 [16]	BC	No hysteresis
Luboń and Tarkowski 2020 [17]	VG	No hysteresis
Mahdi et al., 2021 [39]	VG	Gas-liquid hysteresis
Lysyy et al., 2021 [20]	Field data	No hysteresis
Wang et al., 2022 [40]	CO_2 experiment data	Gas hysteresis
Kanaani et al., 2022 [41]	Field data	No hysteresis
Okoroafor, E.R. et al., 2022 [15]	H_2 experiment data	No hysteresis

water multi-phase flow experiment [36] carried out on a heterogeneous Berea Sandstone rock core at reservoir pressure (10 MPa) and room temperature (18 °C). The Berea Sandstone (Liver) core sample was 17 cm long with a diametere of 3.8 cm and a permeability of 203 mD and porosity of 19.7%. Steady-state drainage and imbibition core-flooding experiments were performed while visualizing the transport of hydrogen and water with the use of a medical X-ray CT scanner, following the techniques described in Krevor et al. [42] and Pini et al. [43]. Fig. 2 shows the set of experimental drainage relative permeability and capillary pressure data, as well as the initial and residual hydrogen saturation, that is used to create our hysteresis model. Here, the initial hydrogen saturation is the hydrogen saturation at the end of drainage, while the residual hydrogen saturation is the hydrogen saturation at the end of imbibition. For a detailed description of the experiment the reader is referred to Boon and Hajibeygi, 2022 [36]. Implications of using this experimental data in our UHS reservoir simulations will be discussed in the forthcoming sections.

Drainage relative permeability models

Theoretical equations are often used to extend the constitutive relationship between relative permeability (k_r), fluid saturation (S), and capillary pressure (P_c) beyond experimentally measured endpoints [42,44]. As shown in Table 1, Brooks-Corey (BC) and Van Genuchten (VG) are two common choices to model $S-k_r-P_c$ relationships in UHS reservoir simulations. In addition, the Brooks-Corey-variable Corey model (BC-vC) has been proposed recently to better fit experimental gas relative permeability data [42]. In this study, we first compare the goodness of fit of BC, VG, and BC-vC equations to match measured k_r-S data from core-flooding and MICP experiments [29,36]. Table 2 provides an overview of the equations of each model as well as values for the input parameters that were used to match the experimental data [45].

In Table 2, the value of the Brooks-Corey geometry factor λ and initial liquid saturation S_{li} are based on the Berea (Liver) sandstone rock core presented in Ni et al. [29]. This rock has similar permeability and porosity values as the Berea (Liver) core used in the core-flooding experiment. Furthermore, the MICP data obtained for the Berea (Liver) core of the study of Ni et al. [29] was used to extend the experimentally measured capillary pressure data over the full range of saturation [36]. We used the technique introduced in Lenhard et al. [46] to calculate an equivalent VG model from the BC model, including the corresponding VG shape factor m (a detailed description of this technique can be found in Appendix A). Both entry capillary pressures in the BC and VG models result from the best fit with experiment data. Fig. 2 provides the resulting drainage relative permeability and capillary pressure curves for each model as well as the experimental data [36]. Fig. 2 shows that neither the BC or VG models can provide a reasonable match with the experimental data. Consequently, we decided to use the BC-vC drainage relative permeability and capillary pressure model for the UHS reservoir simulation, which matches properly the experimental relative permeability and capillary pressure data. It is noteworthy that capillary pressure heterogeneity is not considered in this study, a single capillary pressure curve is used in all simulations.

Gas and liquid relative permeability hysteresis model

Gas relative permeability hysteresis

When a gas-liquid flow in porous media reverses from drainage, where the non-wetting phase is displacing the wetting phase, to imbibition, where the wetting phase is displacing

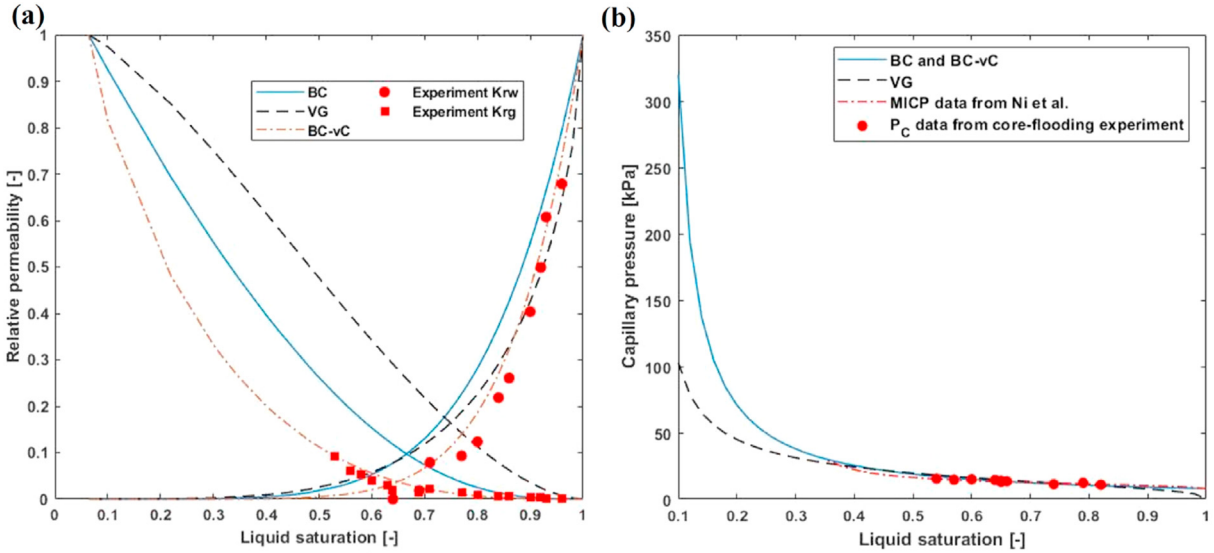

Fig. 2 – (a) Comparison of the three calculated relative permeability models presented in Table 2 with experiment data (red dots and squares, for water and gas, respectively); (b) Drainage capillary pressure curve resulting from BC and VG models and comparison with experimental data (red dots). (For interpretation of the references to color in this figure legend, the reader is referred to the Web version of this article.)

Table 2 – Overview of VG, BC, and BC-vC drainage relative permeability and capillary pressure models.

Model	P_c-S and k_r-S equations	Input values
VG	$P_c = P_0[(S_w^*)^{(1-m)} - 1]^{(1/n)}$	$P_0 = 14$ kPa
	$k_{rl} = (S_w^*)^{1/2}\left[1 - \left(1 - (S_w^*)^{1/m}\right)^{(m)}\right]^2$	$m = 0.62$
	$k_{rg} = (S_g^*)^{1/2}[(1 - (S_w^*)^{1/m})]^{2m}$	
BC	$P_c = P_e(S_w^*)^{-1/\lambda}$	$P_e = 7.9$ kPa
	$k_{rl} = (S_w^*)^{3+2/\lambda}$	$\lambda = 0.88$
	$k_{rg} = (S_g^*)^2[1 - (S_w^*)^{1+2/\lambda}]$	
BC-vC	$P_c = P_e(S_w^*)^{-1/\lambda}$	$P_e = 7.9$ kPa
	$k_{rl} = (S_w^*)^{N_l}$	$\lambda = 0.88$; $N_l = 7$
	$k_{rg} = k_{rg0}(S_g^*)^2[1 - (S_w^*)^{N_g}]$	$N_g = 0.655$; $k_{rg0} = 1$
All models	$S_w^* = \frac{S_l - S_{li}}{1 - S_{li}}; S_g^* = \frac{S_g}{1 - S_{li}}$	$S_{li} = 0.064$

the non-wetting phase, a gas trapping model and a relative permeability scanning model are needed to calculate the end-point gas saturation (residual gas saturation) and the unique scanning path of gas relative permeability connecting the end-point saturation with the saturation at which imbibition starts [33,34]. In this study, the Land gas trapping model [47] is used as follows to calculate the residual gas saturation, i.e.,

$$S_{gt} = \frac{S_{gi}}{1 + CS_{gi}}. \quad (1)$$

here, S_{gi} is the gas saturation at which imbibition starts and C is the Land trapping coefficient. The Killough [48] hysteresis model is used here to calculate the scanning curve based on the starting gas saturation during imbibition. Land and Killough models are routinely used in reservoir simulation studies when considering hysteresis, more explanation about implementing them in reservoir simulations can be found elsewhere [34,49]. To find the Land trapping coefficient, C, we match the experimental gas phase relative permeability hysteresis data from imbibition 1 and imbibition 2 with the calculated gas relative permeability hysteresis model from Land and Killough which resulted in a C value of 2. Fig. 3 (a) shows the gas hysteresis models calculated using Land and Killough models with the imbibition process starting at a gas saturation of 0.47 and 0.38 (corresponding to imbibition experiments 1 and 2 [36], respectively), together with red and dark blue dots representing the experimental gas hysteresis data. Another method to calculate the Land coefficient C is the Initial-Residual (IR) saturation analysis described in Niu et al. [50] and Ni et al. [29], where Land coefficient C is calculated through matching the experimental IR curve, for which the slice average initial and residual saturations from the experiment are being used. Here, to investigate the impact of using these two methods on reservoir simulation, we also calculate a C = 3.2 using average IR data from experiments [36], shown as Fig. 3 (b).

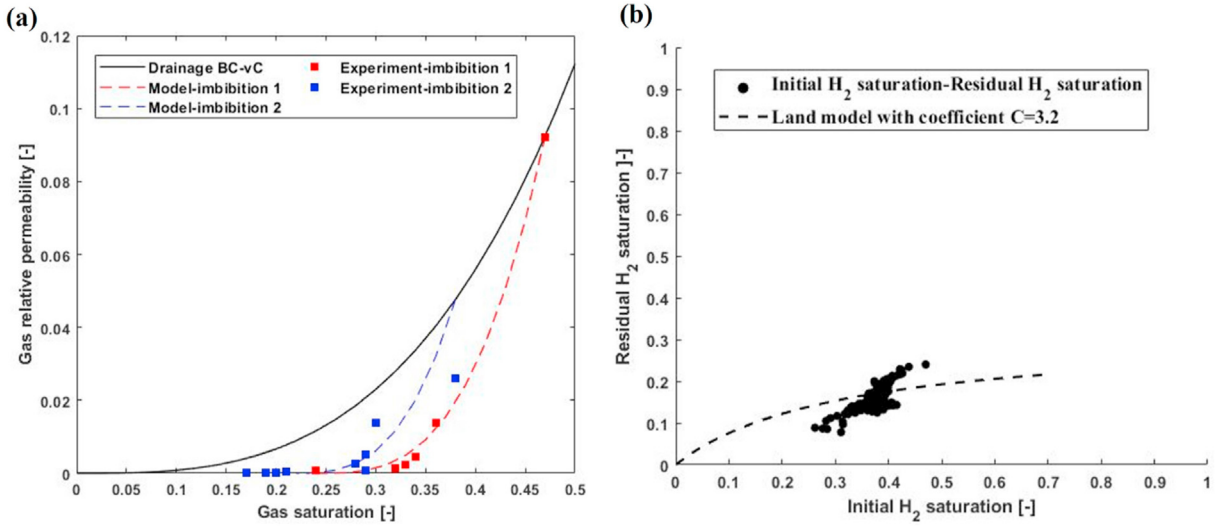

Fig. 3 – (a) Gas relative permeability hysteresis model with C = 2 matching with experimental gas relative permeability hysteresis data [36]; (b) IR plot based on slice average initial and residual saturations [36]. The dashed line shows the Land model curve using coefficient C = 3.2.

To compare the simulation results when using the experimentally measured hydrogen-brine relative permeability curves, which display extremely low imbibition gas relative permeability and strong hysteresis in the wetting phase relative permeability, with other fluids relative permeability curves that do not contain these characteristics, carbon dioxide-brine relative permeability curves from Krevor et al., 2012 [42] are also used in this study. It is noteworthy to mention that the Land coefficient used in Krevor et al., 2012 [42] is 1 and no liquid phase hysteresis is modeled when using these CO_2-brine curves [34]. Accordingly, capillary pressure curve parameters ($S_{li} = 0.11$ and $\lambda = 0.67$) from Krevor et al. [42] are used in the BC-vC model in Table 2 when using relative permeability curves of the CO_2-brine system (P_e is scaled up into 5.6 kPa for the hydrogen-brine system using Young-Laplace scaling [36]). Finally, capillary pressure hysteresis is not considered in this study as the scale of reservoir simulation is much larger than the characteristic capillary dimension [51] and related experimental hysteresis capillary pressure data is not available [36].

Liquid relative permeability hysteresis

When modelling liquid relative permeability hysteresis, a 'maximum' liquid relative permeability hysteresis curve which starts from the irreducible liquid saturation (S_{li}) to the liquid saturation at maximum residual gas saturation ($1 - S_{grmax}$) is usually prescribed. The imbibition relative permeability at liquid saturation larger than S_{li} will be interpolated using scanning curves. In this study, the Killough model [48] is used to interpolate between experimental data matched to maximum liquid relative permeability hysteresis curve (orange curve in Fig. 4) and the drainage liquid relative permeability curve (blue curve in Fig. 4). It is noteworthy that we did not find a suitable model to match with our experimental imbibition 1 liquid relative permeability hysteresis data. Therefore, the orange curve in Fig. 4 is a representation of the tabulated data that we incorporated into our simulations. The reason for this is to make sure that the input liquid relative permeability hysteresis model will not cross over the drainage relative permeability model.

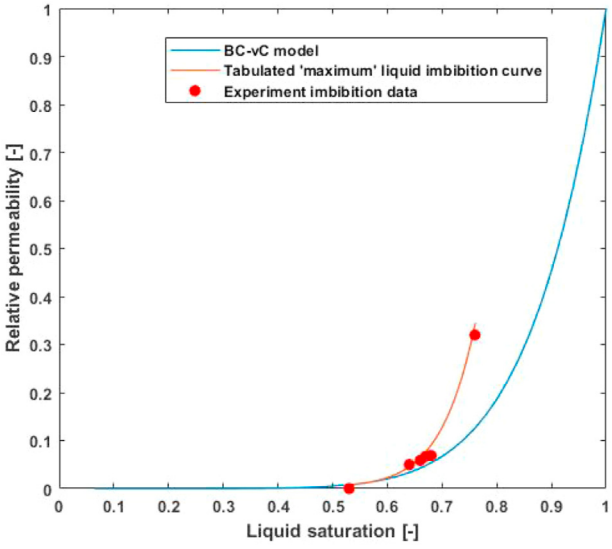

Fig. 4 – Liquid relative permeability hysteresis model; blue curve represents drainage relative permeability; orange curve represents tabulated 'maximum' liquid imbibition relative permeability curve; red dots represent experiment data. (For interpretation of the references to color in this figure legend, the reader is referred to the Web version of this article.)

Numerical simulations

A commercial compositional numerical simulator [52] is used to perform a series of simulations to assess the effect of gas-liquid relative permeability hysteresis on the hydrogen and water production during UHS cyclic operations.

Reservoir description

The modelling domain is based on the open-source model and field data from a commercial depleted gas reservoir in the Otway Basin, Australia called Fenton Creek. In 2020, the Victoria Geological Survey conducted a research program called Victoria Gas to investigate the potential of gas reservoirs in the Port Campbell region of the Otway Basin for storing natural gas [53]. Fenton Creek is a small fault-bounded water-gas reservoir with very high permeability and porosity, and therefore is a good candidate for gas storage. For this reason static geological and dynamic models of the Fenton Creek gas reservoir were built, respectively. The models are publicly available for download (http://earthresources.efirst.com.au/). Fig. 5 displays the depth contour map of this gas reservoir. A single production well (Fenton Creek-1) is located at the lower crest of the reservoir and the gas reservoir is bounded by two major faults. This model has been modified and adapted to the purpose of this study. In our model, in order to produce hydrogen from the crest of the reservoir where it easily accumulates due to buoyancy, both an injection and production well were placed at the top crest of the anticline. Another reason for this new well scenario is that, wells near the faults could facilitate monitoring the pressure variance during cyclic operation.

The Fenton Creek gas reservoir is discretized into 60*18*30 grid blocks, of which 20,500 are active. The average grid size is 40*40*1.75 *m* which is comparable to other UHS reservoir-scale simulation studies [15,16,54]. Moreover, to study the effect of grid size on the results, test simulations were conducted. It was found that grid sizes within practicable range did not significantly impact the results, more details are presented in appendix B. The reservoir is at a moderate depth around 1500 m. The temperature gradient is 30.4 °C/km. A reservoir pressure of 15,030 kPa is measured at the water-gas contact. Under such condition, the phase density and viscosity calculated by the simulator through the revised Peng-Robinson equations [55] (after regression with experimental data) are within 0.5% (for hydrogen-methane mixture density) and 7% (for hydrogen-methane mixture viscosity) of values given in the literature [56,57]. As shown in Fig. 5, the reservoir is bounded and sealed by closed faults and supported by a bottom aquifer with a volume of $88*10^6 m^3$ during primary production of the reservoir [53]. Fig. 6 shows a 3D view of the model with the well location and water saturation.

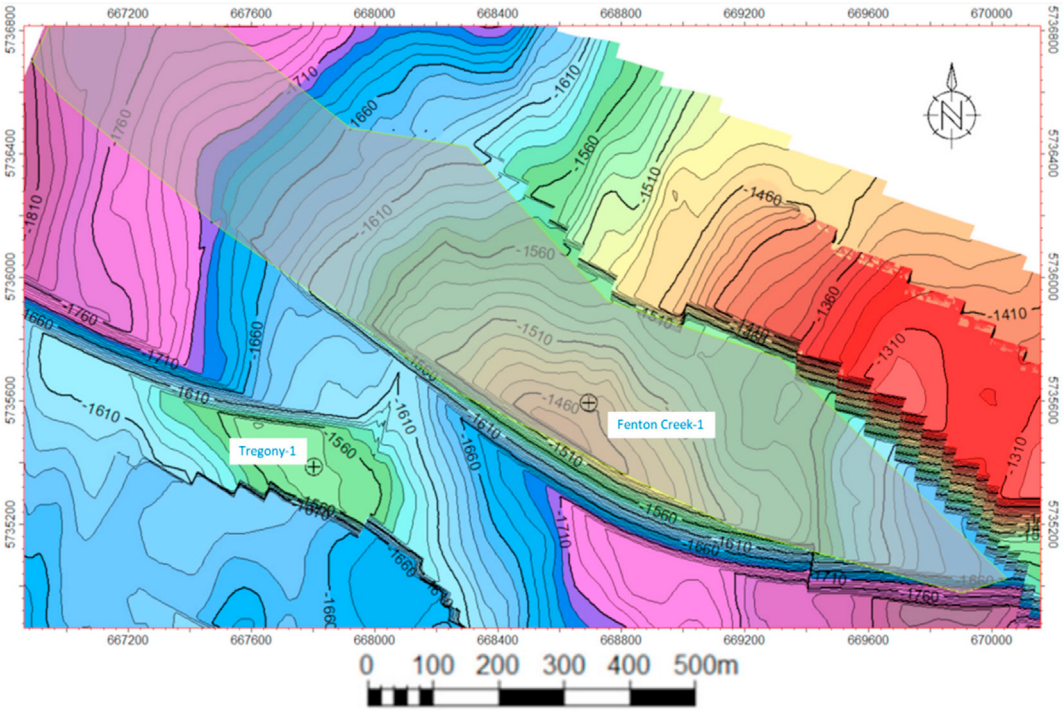

Fig. 5 – The original areal view of the depth contour map of the Fenton Creek gas reservoir; the gas reservoir region is shaded in grey and the Fenton Creek-1 production well location is marked by a cross.

Well logs show that the Fenton Creek consists for around 80–90% of sandstone in the gas cap. The sandstone facies of Fenton Creek is highly permeable with average permeability above 1000 mD as evidenced by the core permeability-porosity cross plot of the field [38]. However, the Berea sandstone core sample that was used to measure the hydrogen-brine relative permeability has a permeability and porosity of only 203 mD and 0.197, respectively. For this reason, a sandstone facies porosity-permeability transformation function in the model is revised to make the reservoir average permeability to be 218 mD which is close to the core sample in the experiment. The shale facies (low permeable facies) in the model is still using the original porosity, permeability, relative permeability, and capillary pressure data from the field. The ratio between horizontal permeability and vertical permeability in our model is 10. Fig. 7 presents a resulting areal view of the horizontal permeability distribution of the model.

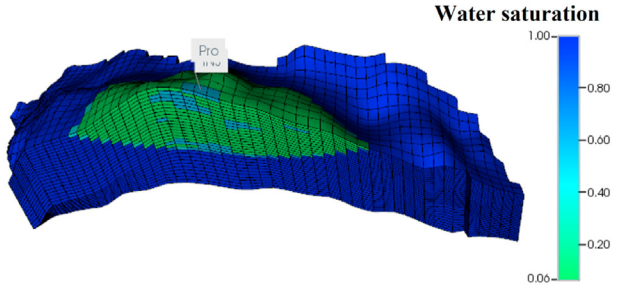

Fig. 6 – 3D view of the geological model with a water saturation map (initial state, before primary production) and well location (injection well and production well are in the same place).

Simulation setup

There are three stages in our simulation, (1) primary production of methane from the reservoir, (2) initial injection of cushion gas using pure hydrogen, followed by (3) 10 UHS cyclic operations. The injection rate and production rate in each cycle are the same within a single case. Note that depending on well constraints, a target injection/production rate may not be achievable. The period of each cycle is 1 year for all the cases. Two injection/production schemes are used and the same total volume of injected/produced hydrogen is maintained in all cases. In the '6 month–6 month' scheme, hydrogen is injected for six consecutive months and then produced for the next six months and this is repeated for 10 cycles (i.e. a total duration of operations of 10 years). The other is the '3 month–3 month' scheme with injection for 3 months, idleness (shut-in) for 3 months, production for 3 months, then idleness for another 3 months and this is repeated for 10 cyclic operations (total operation period of 10 years). If the injection/production rate is doubled, the 6 month–6 month scheme will change to the 3 month–3 month scheme to make the total targeted injection/production consistent.

To test the effects of hysteresis on the performance of UHS and study its underlying mechanism in different scenarios, 5 cases were designed: three cases investigate the effects of gas-liquid hysteresis and the other two cases examine hysteresis effects under different cyclic injection/production rates (see Table 3). Hereafter, the mention of gas saturation refers to the hydrogen gas phase. Case 1 models UHS cyclic operations

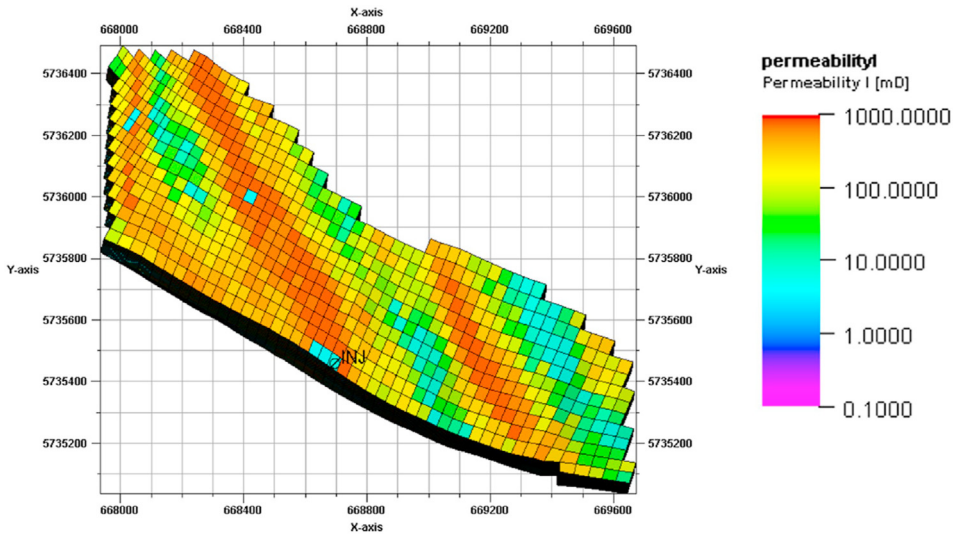

Fig. 7 – The areal view of the permeability distribution after adjusting the porosity-permeability relationship to the specific characteristics of this study.

without hysteresis and follows a moderate injection/production rate ($0.5*10^6 m^3/day$) with a 6 month–6 month scheme. Case 2 includes only gas hysteresis while case 3 models gas and liquid hysteresis, both under the same injection/production scenario as case 1. Case 4 tests an extreme injection/production rate ($1.0*10^6 m^3/day$) with a 3 month–3 month scheme. In contrast, Case 5 tests for low injection/production rate ($0.15*10^6 m^3/day$) with the 6 month–6 month scheme. The simulation schedule and injection/production rate are set based on production history and simulation scenarios from the Victoria Gas Program (injection/production rate ranges from $0.35*10^6 m^3/day$ to $0.7*10^6 m^3/day$) [53]. These injection and production periods are a bit longer than those used in other UHS reservoir simulation studies [16,19,20], to reach the limit of the reservoir to better contrast the cases.

After the effects and mechanism from hydrogen relative permeability hysteresis on UHS performance assessment have been revealed and understood via testing case 1 to 5, differences that arise from using different relative permeability curves including imbibition from various fluid systems can be tested and explained. The effects from using different methods to calculate the Land coefficient C on UHS reservoir simulations is investigated through case 6 where the Land trapping coefficient (C = 3.2) determined from the experimental IR curve is used. Finally, the difference between using experimental hydrogen relative permeability curves, which display extremely low imbibition gas relative permeability and strong hysteresis in the wetting phase relative permeability, with other fluids relative permeability curves that do not contain these characteristics, is studied by case 7. Instead of using the relative permeability model constructed for this study, case 7 uses experimental relative permeability curves for the CO_2-brine system from Krevor et al., 2012 [42], as shown in Fig. 1. Case 6 and 7 only differentiate themselves from case 3 by Land coefficient and relative permeability curves, respectively. Also, it is noteworthy that all the tested cases use the same pressure constraints at the wells. The maximum bottom hole pressure for the injection well is set to 15,000 kPa to assure that reservoir pressure does not exceed the initial (gas primary production stage) reservoir pressure, and the minimum bottom hole pressure for the production well is set to 5000 kPa to maintain the minimum pressure

Table 3 – Overview and description of each simulation case.

Case	Hysteresis	Inj/Pro rate [$10^6 m^3/day$]	Inj/Pro duration	Land coefficient
Cases for studying hysteresis mechanisms				
Relative permeability curves from Boon et al. [36]				
1	No hysteresis	0.5	6 month-6month	2
2	Gas hysteresis	0.5	6 month-6month	2
3	Gas-liquid hysteresis	0.5	6 month-6month	2
4	Gas-liquid hysteresis	1.0	3 month-3month	2
5	Gas-liquid hysteresis	0.15	6 month-6month	2
6	Gas-liquid hysteresis	0.5	6 month-6month	3.2
Cases for studying different relative permeability				
Relative permeability curves from Krevor et al. [42]				
7	Gas hysteresis	0.5	6 month-6month	1

required for transportation and processing downstream [53]. Table 3 provides an overview and description of each simulation case.

Results and discussion

Effects of gas and liquid relative permeability hysteresis

The effects of relative permeability hysteresis can be dramatic as can be seen from the prediction of gas saturation, cumulative hydrogen production, and cumulative water production.

In case 1, relative permeability is reversible and only drainage relative permeability is modeled. While case 3 models both gas and liquid relative permeability hysteresis, case 2 considers only gas relative permeability hysteresis to investigate the effects caused by liquid relative permeability hysteresis.

Fig. 8 compares the hydrogen gas saturation map between case 1 (no hysteresis), case 2 (only gas hysteresis), and case 3 (gas-liquid hysteresis) at the end of 10 cyclic operations. In case 1, in the absence of hysteresis, a sharp gas-water contact moves up towards the production well during production periods, leaving a residual gas plume with gas saturation ranging between 0 and 0.2 below the gas-water contact. This plume exhibits discontinuities that reflect the permeability distribution (not shown) confirming that liquid bypassing is causing the residual trapping of the gas phase.

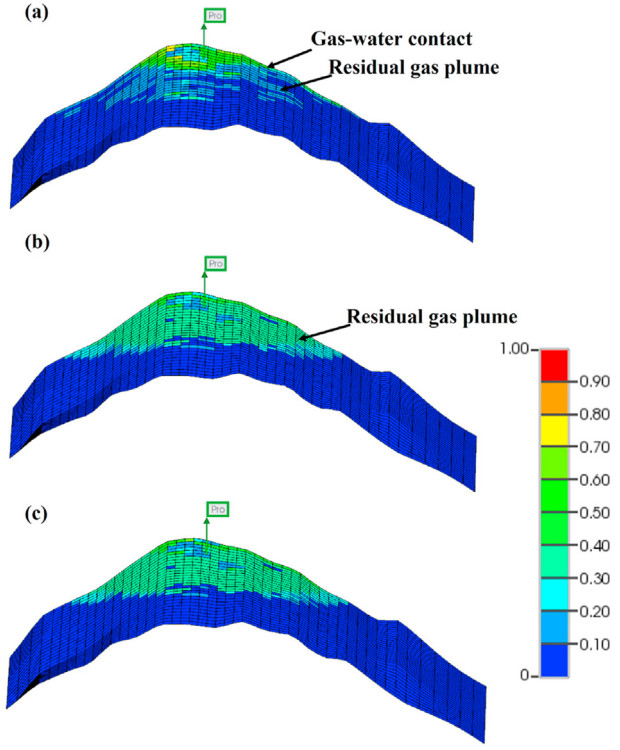

Fig. 8 – Gas saturation map by the end of 10 cyclic operations of (a) case 1, no hysteresis; (b) case 2, gas hysteresis; (c) case 3, gas-liquid hysteresis.

The gas saturation in cases 2 and 3 are entirely different. Due to hysteresis and gas trapping, a residual gas plume forms below the gas-water contact at the fringe of the shrinking gas cap during production periods. The gas saturation in this residual gas plume ranges between 0.2 and 0.35, corresponding to the residual gas saturation obtained when imbibition starts at the beginning of primary production (first stage of simulation), using the Land model. As a result, the gas-water contact is very 'fuzzy' and there is little mobile/free gas in the reservoir. A similar gas saturation map has been observed in another UHS simulation study where gas relative permeability hysteresis is considered [40]. The exclusion of liquid relative permeability hysteresis does not cause a distinct between cases 2 and 3, as can be seen comparing Fig. 8 (b) and (c). The reason for this is that liquid relative permeability hysteresis will not change the end-point saturation, instead it will only change the relative permeability of the liquid phase.

These hysteresis effects will affect injectivity and productivity during UHS cyclic operations. Fig. 9 shows the injection (negative) and production rate (positive) history of the three cases. All three cases are not able to reach the target gas rate during the whole 10 cycles of operation. Case 1 delivers the target gas rate but it declines after several months because well pressure constraints are reached. On the other hand, case 2 and 3 which consider hysteresis, can hardly reach the target gas rate of $0.5*10^6 m^3/day$ already in the first injection cycle. This is because hysteresis immobilises a large fraction of gas in the reservoir, leading to very low gas relative permeability during injection and production. Liquid hysteresis is excluded in case 2 and cyclic injectivity and productivity is lower than that of case 3. The reason can be seen in Fig. 10 which shows cumulative hydrogen (a) and water (b) production for cases 1, 2, and 3. In case 2 less water is produced during the first cycle due to the lower liquid relative permeability. As a result, there is less space for mobile gas flow in the reservoir in consecutive cycles. Consequently, the difference between the cumulative

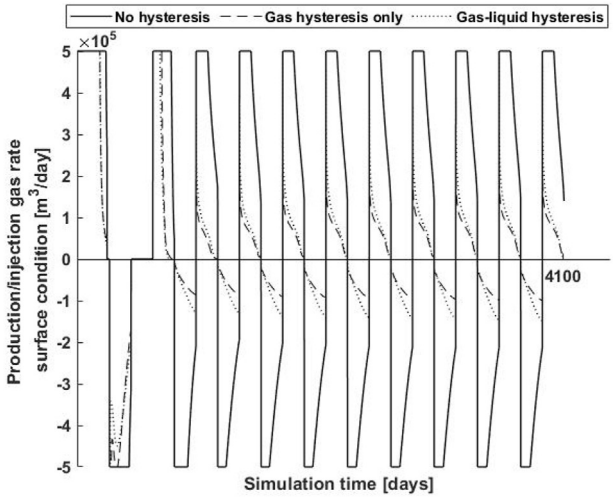

Fig. 9 – Volumetric gas production (positive) and injection (negative) rate at surface condition for case 1 (no hysteresis); case 2 (gas hysteresis only); case 3 (both gas-liquid hysteresis).

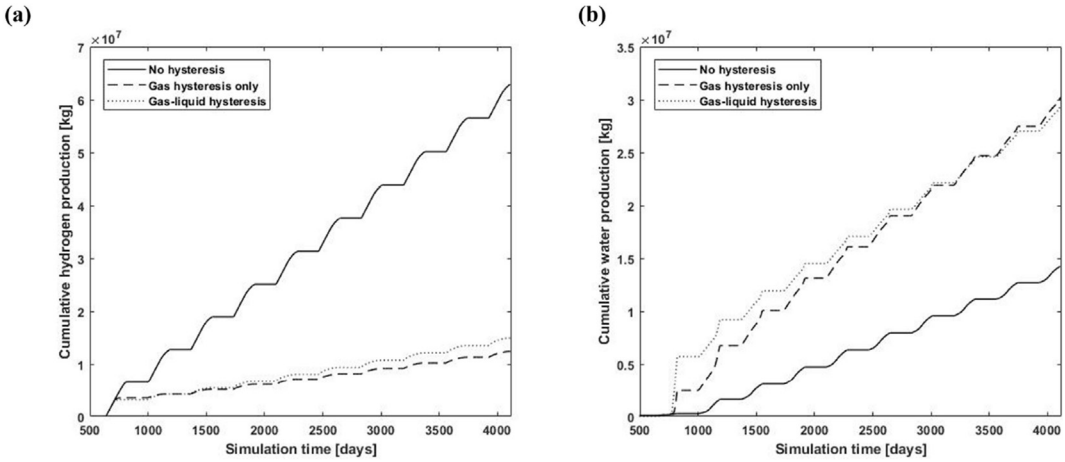

Fig. 10 – Cumulative production history of (a) hydrogen and (b) water for case 1, 2, and 3.

hydrogen and water production of case 2 and 3 becomes larger with each production cycle.

The comparison of case 1 with case 2 and 3 shows that the relative permeability hysteresis starts to affect the simulation of UHS operations from the start of the primary production of the reservoir. For an aquifer-driven gas reservoir as used in this study, hysteresis and gas trapping determine the remaining space in the reservoir for storing hydrogen. Simulations show that hysteresis will have a negative impact on the injectivity and productivity of hydrogen gas. Figs. 9 and 10 show that failing to consider the relative permeability hysteresis effects will lead to an overestimate by 338% for the cumulative hydrogen production and an underestimate by 54% for the cumulative water production after 10 cyclic operation periods, respectively. Liquid hysteresis is also important to consider as it provides space in the reservoir for hydrogen storage in the first cycle, resulting in a 17% increase in cumulative hydrogen production and 2.5% decrease in water production by the end of the 10 cycles, and these differences will keep growing with increasing number of cycles. Therefore, correct and accurate characterization of relative permeability including imbibition is necessary for reservoir-scale UHS injectivity and productivity assessment as the uncertainty brought by hysteresis will be exaggerated over time in simulations.

Effects of injection/production rate

Next the performance of UHS under different target injection/production rates when accounting for hysteresis is investigated. Results from cases 3, 4, and 5 are compared. In case 3 and 4, the same target volume of gas is cycled during different cyclic schemes (3 months–3 months and 6 months–6 months), while case 5 targets a lower injection/production rate under the same cyclic scheme as case 3 (6 months–6 months).

The resulting gas injection/production rate from case 3, 4, and 5 are shown in Fig. 11. Clearly, comparing the red curve (case 4, high injection/production rate) with the black curve (case 3, medium injection/production rate), increasing the target injection/production rate does not result in a better cyclic performance because the injectivity and productivity are impaired due to hysteresis. Both case 3 and 4 cannot reach the target injection or production rate for any continuous period. In contrast, at a lower target injection/production rate (case 5), and a lower total target volume of gas per cycle ($0.15*10^6 m^3/day$ compared to $0.5*10^6 m^3/day$), a better injection and production performance is achieved. The low injection/production rate case (case 5, dark blue curve in Fig. 11) achieves the target production/injection in all cycles. The reason for these results is explained in the following.

A high target injection/production rate is expected to cause higher gas pressure brought by a higher bottom-hole pressure and thus an increase in gas saturation. Consequently, the gas relative permeability would increase during the cyclic operations and therefore injectivity and productivity. However, from Fig. 12 which shows the gas saturation variation in two

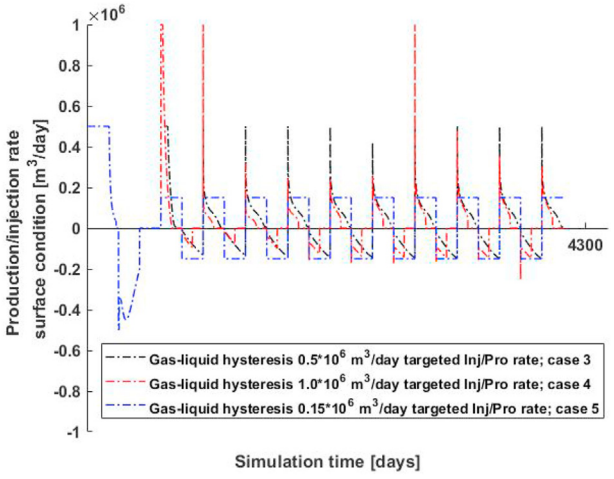

Fig. 11 – Gas production/injection rate at surface condition of medium injection/production rate case 3 (black curve), high injection/production rate case 4 (red curve), and low injection/production rate case 5 (dark blue curve). (For interpretation of the references to color in this figure legend, the reader is referred to the Web version of this article.)

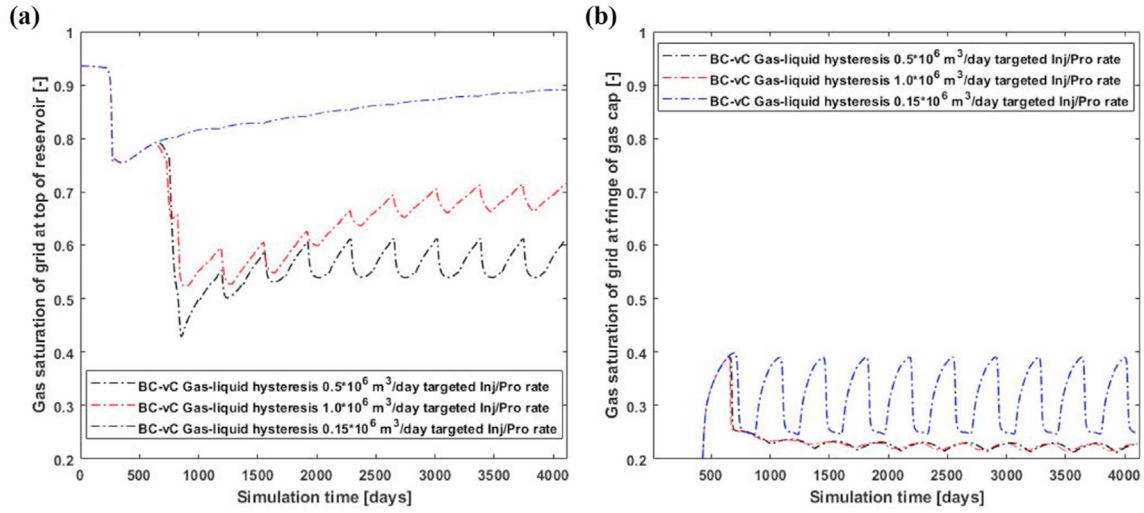

Fig. 12 – Gas saturation variation during cyclic operations of a grid block at (a) top of the reservoir near wellbore region, coordinates (31,2,1); (b) fringe of gas cap, coordinates (46,2,3); for the medium (case 3 - black curve), high (case 4 - red curve), and low (case 5 - dark blue curve) injection/production rates, respectively. (For interpretation of the references to color in this figure legend, the reader is referred to the Web version of this article.)

grid blocks at the top of the reservoir and at fringe of the gas cap, respectively, in cases 3, 4, and 5, it can be seen that high injection/production rate (red curve) does not 'produce' more mobile gas. At the top of the reservoir (Fig. 12a), the gas saturation does increase compared to the medium injection/production rate (black curve) as expected during the first several cycles. However, due to the upward migration of hydrogen gas because of gravity (buoyancy), the amount of mobile gas at the fringe of the gas cap decreases (Fig. 12b - both for case 3 and 4). This gravity driven upward movement of gas ends when the injection pressure, and therefore the gas, can not effectively spread to the fringe of the gas cap. In these circumstances, several percent higher gas saturation at the top of the reservoir will not bring higher productivity, as shown in Fig. 11 (red curve compared to black curve). Simply increasing the target injection/production rate and bottom-hole pressure will not release the mobile gas accumulated at the top of the gas cap more effectively (Fig. 12a red curve and black curve) because well constraints are reached and then injectivity and productivity can not reach target values. Instead, due to the less effective pressure spread brought by higher bottom hole pressure, less gas is mobile in case 4 than case 3 during the last several cycles.

The situation is different when it comes to low target injection/production rate as in case 5 (dark blue curve in Fig. 12). Because of the lower bottom-hole pressure, pressure and gas can be delivered to the fringe of the gas reservoir (Fig. 11b where the dark blue curve shows more mobile gas compared to the other cases). Consequently, the pressure spreads better and releases the mobile gas at the fringe of the gas cap during production periods and delivers them back, leading to higher injectivity and productivity for case 5. Similar to the high injection/production rate case, the gas saturation at the top of the reservoir (Fig. 12a dark blue curve) increases when more gas is injected into the reservoir and accumulates at the top.

Effects of different hysteresis models

Higher gas relative permeability and less trapping during imbibition is brought by using Land coefficient C = 3.2 (case 6) instead of C = 2 and results in a better gas and pressure spread similar to what happens in case 5, compared to case 3. Fig. 13 shows the difference in the relative permeability hysteresis model and gas saturation at the top and bottom of the gas cap between the two models. Clearly, when gas relative permeability is higher, more methane gas is produced out from the top of the gas cap by the end of 252 days (stage 1, Fig. 13b). As a result, more space is available at the top of the gas cap for the injected hydrogen gas in case 6 compared to case 3. For this reason, less hydrogen gas reaches the bottom of the gas cap and more gas stays at the top of the reservoir for case 6 during initial injection (around 500 days in Fig. 13b). Due to the better spread of gas and pressure for case 6, the gas cap keeps expanding during cyclic operations and the gas saturation at the bottom of the gas cap also keeps increasing. In contrast, the hydrogen gas cannot reach the bottom of the gas cap in case 3 after initial injection due to smaller gas relative permeability and the less effective pressure spread, decreasing the amount of mobile gas available after each cycle.

Comparison with other fluids system

Despite the fact that the experimental CO_2-brine relative permeability curves that were used for case 7, shown in Fig. 1, have a larger gas relative permeability (both drainage and imbibition) and drainage liquid phase relative permeability, simulating UHS using these CO_2-brine relative permeability curves leads to a much smaller cumulative hydrogen production after 10 cyclic operations.

Fig. 14 (a) shows the cumulative hydrogen production history during cyclic operations of case 3 and 7. The hydrogen production of case 3 is higher than that of case 7 already from

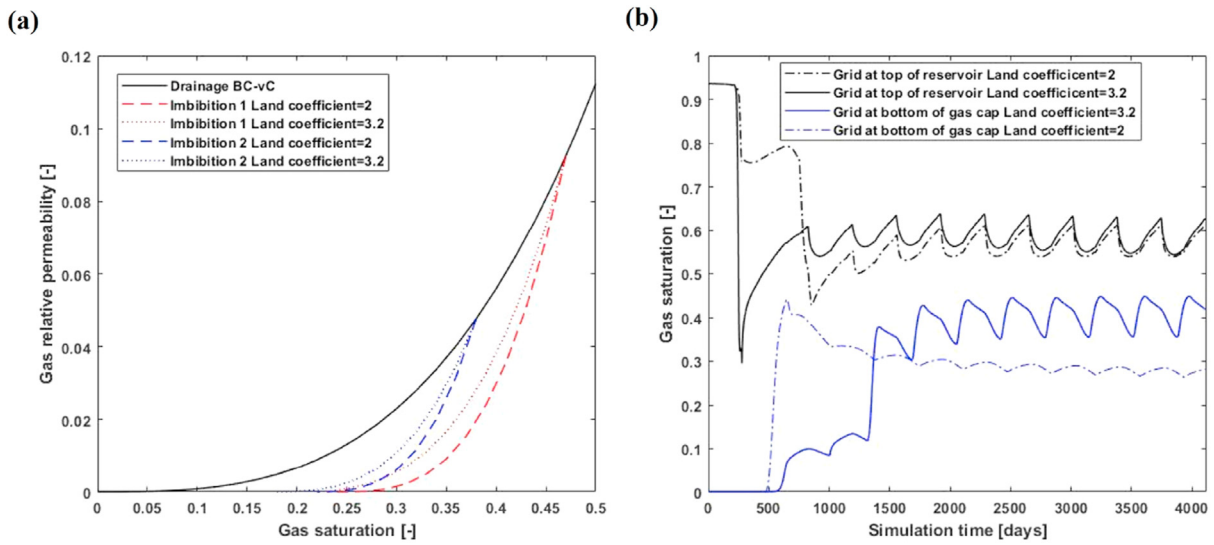

Fig. 13 – (a) Comparison between calculated gas relative permeability hysteresis model with Land coefficient C = 2 (dashed curve) and C = 3.2 (dotted curve); (b) Gas saturation variation during cyclic operations at a grid block at the top of the reservoir near wellbore region (black curve), coordinates (31,2,1); at the fringe of the gas cap (dark blue curve), coordinates (48,2,1); in case 3 and 6. (For interpretation of the references to color in this figure legend, the reader is referred to the Web version of this article.)

the first cycle and the difference between them keeps increasing till the end of the simulation. Based on the results from previous cases, this is because the liquid phase relative permeability during imbibition for case 7 is much lower than case 3, making it hard for the liquid phase to be produced or displaced by injected hydrogen. Fig. 14 (b) presents the gas saturation variation during simulation. Due to the larger drainage relative permeability, the gas saturation does reach a higher level during the initial injection stage compared to case 3, but the range of gas saturation variation of case 7 is much smaller. This is brought by the lower liquid phase relative permeability during imbibition and subsequent poorer sweep of pressure and injected hydrogen which is consistent with the observations from previous cases.

Overview of all cases

Table 4 gives an overview of the key differences in the results for the cases in this study in terms of cumulative hydrogen production, hydrogen recovery, and cumulative water

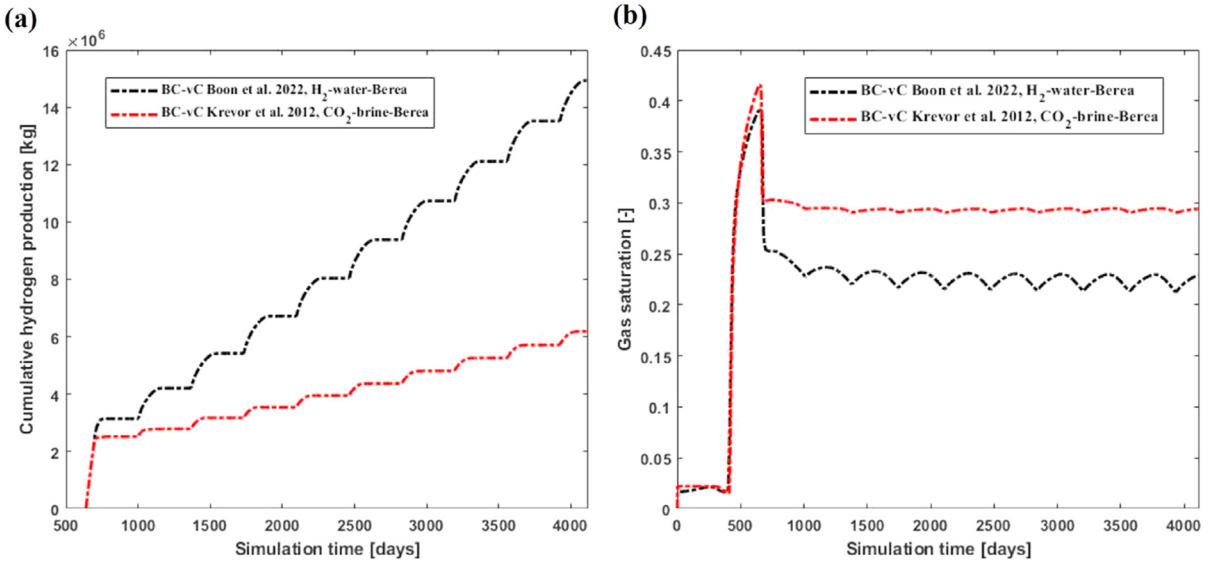

Fig. 14 – (a) Cumulative hydrogen production history of case 3 (black curve, H_2-brine relative permeability, with both gas and liquid phase hysteresis) and 7 (red curve, CO_2-brine relative permeability, only gas phase hysteresis); (b) Gas saturation variation during cyclic operations at the fringe of the gas cap, coordinates (46,2,3); in case 3 and 7. (For interpretation of the references to color in this figure legend, the reader is referred to the Web version of this article.)

Table 4 – Overview of results from all cases.

Case	Sensitivity	Cumulative hydrogen production (kg)	Hydrogen recovery (%)	Cumulative water production (kg)
1	–	$6.288*10^7$	97.87	$1.424*10^7$
2	Gas hysteresis	$1.239*10^7$	81.78	$3.022*10^7$
3	Gas-liquid hysteresis	$1.493*10^7$	83.84	$2.948*10^7$
4	High injection/production rate	$0.962*10^7$	78.25	$1.136*10^7$
5	Low injection/production rate	$2.218*10^7$	83.95	$1.377*10^7$
6	Land coefficient	$3.229*10^7$	91.08	$2.274*10^7$
7	CO_2 relative permeability	$0.618*10^6$	67.00	$0.003*10^7$

production. Comparing case 1 with 2 (with hysteresis), as a result of gas hysteresis, a large amount of gas is trapped behind the gas-water contact when the gas cap is shrinking towards the production well, thus decreasing the cumulative hydrogen production and hydrogen recovery. Meanwhile, the inclusion of liquid hysteresis (case 3) improves this situation by increasing the relative permeability of the liquid phase, allowing more gas to be injected (17.5% more gas is injected in case 3 compared to case 2) and produced from the reservoir. A fraction of this injected gas will in return get trapped in the reservoir and decrease the water relative permeability during later cycles and finally result in less cumulative water production. Since the medium injection/production rate (case 2 and 3) is difficult to reach, simply increasing the target injection/production rate and shortening the cycle duration (case 4) will only increase the value of gas saturation at the top of the reservoir (Fig. 11a red curve). Such a scenario cannot effectively enlarge the range of pressure and gas saturation during cyclic operations (Fig. 11a, compare black and dark blue curve). Instead, the pressure and gas saturation variation range decreases because of the shorter cycle and higher bottom-hole pressure, as well as the cumulative water and hydrogen production (Table 4). In contrast, a lower target injection/production rate and a higher gas relative permeability hysteresis model, require a lower bottom hole pressure difference, leading to a better spread of both pressure and gas. When more of the injected gas is trapped in the reservoir due to hysteresis (case 5 and 6, Figs. 11a and b dark blue curve, and Fig. 12b), the liquid relative permeability is decreased, resulting in a reduction of the cumulative water production (case 5 has the second lowest water production in all cases, case 6 has 29% less water production under same injection/production rate as case 3). Therefore, from the comparison of cases 3, 4, 5, and 6, it can be concluded that it is the achievable range of pressure and gas saturation that provides effective UHS injectivity and productivity. Hydrogen relative permeability hysteresis decreases injectivity and productivity by trapping the injected hydrogen and connate natural gas, diminishing the amount of mobile gas, and decreasing the gas phase relative permeability. The above shows that incorporating accurate IR data and relative permeability hysteresis data in modelling are equally important for UHS reservoir simulation, as they affect the gas saturation and pressure variations during UHS cyclic operations, respectively.

The results of the comparison between case 3 and 7 emphasize the importance of using experimentally measured hydrogen-brine relative permeability including imbibition when simulating UHS at reservoir-scale. Implementing relative permeability curves from other fluid systems will cause uncertainty in terms of gas saturation and up to 141% underestimation on cumulative hydrogen production. As such, more experimental and numerical studies are needed to further study the unique characteristics of hydrogen-brine relative permeability including imbibition.

The effects of experimentally measured hydrogen relative permeability hysteresis on UHS resulting from the simulations described above are associated with several assumptions and particularities of the selected reservoir. The relative permeability in this study is fixed. Part of the effect of porosity and permeability variations on relative permeability are considered naturally through the heterogeneous absolute permeability (recall that the effective permeability to a fluid is the product of absolute permeability and relative permeability of the fluid). However, a more complete model would incorporate variations in relative permeability according to the permeability and porosity variation as well. Reservoir simulation in this study only considers gravity, capillary, and viscous forces, so flow behaviors may change when more physics are included. For example, when geochemical reactions are considered and there are sensitive minerals present in the reservoir, the petrophysical properties of rock may change during UHS cyclic operations [23,58], which may affect UHS projects. Mechanical deformation under fluctuating pore pressure is also another important physical processes that may alter the hydrodynamics of the UHS projects [59,60]. In this study, the reservoir for hydrogen storage is based on the depletion of a hydrocarbon gas reservoir. Also, the experimentally measured hydrogen gas phase relative permeability used in this study is very low (most below 0.1) which is partially consistent with other hydrogen-brine relative permeability experiment studies [37,44]. If a higher gas phase relative permeability is used (e.g. the case 6 and 7 in this study), the inclusion of both gas-liquid hysteresis, compared to cases without them, may lead to estimates of higher injectivity and productivity for UHS projects. However, due to hysteresis gas trapping, the recovery will still be lower than without it (case 3 and 7) [61]. Therefore, the comparison between case 3, 6, and 7 in this study may serve as a starting point of discussion on how different relative permeability models (including hysteresis) will affect the simulated performance of UHS projects. Lastly, the depleted gas reservoir in this study is a quite small generic water-gas reservoir. This setting leads to more water production and lower achievable injection/production rate compared to larger oil and gas reservoirs where expansion or weak aquifer drive dominates. Indeed, it would have been more realistic to simulate primary production (simulation stage 1) using gas-brine relative permeability from the depleted gas field, instead

of hydrogen-brine relative permeability curves. However, the commercial simulator that was used did not allow it. Our study might underestimate the gas production during the primary production stage or overestimate the gas production during the UHS cyclic operation stage. Furthermore, the multiphase flow behavior in the transition zone where hydrogen and cushion gas are mixing is still unknown. We recommend related research to be conducted in the future.

Conclusion

Experimentally measured hydrogen relative permeability especially hysteresis curves show distinct characteristics compared with that of other fluid systems (gas-water [30] and CO_2-brine [42]). Such hysteresis in the gas-liquid relative permeability of the hydrogen-brine-rock system has profound effects on the prediction of saturation distribution, hydrogen production, and water production for UHS projects conducted through reservoir-scale simulations. The main effects are summarized as follows.

1. First of all, accounting for gas relative permeability hysteresis during simulation of the UHS process is essential to accurately assess the injectivity and productivity of a UHS project. As a result of gas trapping, less of the pore space is available for the mobile injected hydrogen gas which decreases the gas phase relative permeability and consequently the injectivity and productivity. In certain scenarios, failing to consider gas relative permeability hysteresis will cause an overestimate by up to 338% of cumulative hydrogen production.
2. Accounting for liquid hysteresis in UHS simulation increases the liquid phase relative permeability which makes it easier for the injected hydrogen phase to displace the liquid phase. However, the trapping of gas will eventually decrease the liquid phase relative permeability at the fringe of the gas cap (compared to less trapped gas saturation in other scenarios), and the ultimate water production will be less compared to cases that do not consider liquid hysteresis.
3. The effects from gas and liquid relative permeability hysteresis would be different depending on specific UHS scenarios. More specifically, when gas phase relative permeability is very low, increasing the injection/production rate will only increase the gas saturation. At the same time, it will also decrease the range of gas saturation variation during the cyclic production period, due to the shorter production periods and less effective pressure spreads. Under these circumstances, gas phase hysteresis is more important than liquid hysteresis since it further decreases the gas relative permeability and consequently the hydrogen injectivity. In contrast, when gas relative permeability is enough to provide the target injection/production rate after considering gas hysteresis, liquid hysteresis is more important. This is because it can improve the displacement of liquid phase by injected gas phase, increasing the variation range of gas saturation in the whole gas cap region and subsequent productivity during cyclic operations.
4. Relative permeability curves obtained for other fluid systems are proven to be not suitable for acting as proxy of hydrogen-brine relative permeability curves (including imbibition). The strong liquid phase relative permeability hysteresis for hydrogen-brine system provides 141% more productivity even with much smaller gas phase relative permeability compared to that of other fluid systems. When assessing UHS performance at reservoir-scale with strong aquifer support, the use of experimentally derived hydrogen-brine relative permeability curves including imbibition is recommended.

CRediT authorship contribution statement

Zhenkai Bo: Investigation, Methodology, Writing-original draft; Maartje Boon: Review&Editing, Methodology; Hadi Hajibeygi: Review&Editing, Conceptualization, Funding acquisition, Supervision; Suzanne Hurter: Review&Editing, Funding acquisition, Administration, Supervision.

Declaration of competing interest

The authors declare that they have no known competing financial interests or personal relationships that could have appeared to influence the work reported in this paper.

Acknowledgements

This research is a result of collaboration between the University of Queensland (UQ), Delft University of Technology (TU Delft), and the Netherlands Organisation for Applied Scientific Research (TNO) through The 1st International Summer School on Underground Hydrogen Storage held at TU Delft in 2022. The Centre for Natural Gas at UQ and ADMIRE group at TU Delft are acknowledged for the travel funds for Zhenkai. In addition, Zhenkai acknowledges the University of Queensland and Energi Simulation for the University of Queensland Research Training Stipend and Research Higher Degree Top Up Scholarships. Hadi Hajibeygi also acknowledges the support of Energi Simulation through the chair in Subsurface Storage and Multiscale Modeling at TU Delft.

Appendix A. Supplementary data

Supplementary data to this article can be found online at https://doi.org/10.1016/j.ijhydene.2022.12.270.

REFERENCES

[1] Agreement P, United nations. United nations treaty. Collections 2015:1–27.
[2] Energy E. A strategy for competitive, sustainable and secure energy. 2020.
[3] Schiebahn S, Grube T, Robinius M, Tietze V, Kumar B, Stolten D. Power to gas: technological overview, systems

analysis and economic assessment for a case study in Germany. Int J Hydrogen Energy 2015;40(12):4285–94.
[4] Wu Y, Charlesworth L, Maglaya I, Idros MN, Li M, Burdyny T, Wang G, Rufford TE. Mitigating electrolyte flooding for electrochemical co2 reduction via infiltration of hydrophobic particles in a gas diffusion layer. ACS Energy Lett 2022;7(9):2884–92.
[5] Tang K, Meyer Q, White R, Armstrong RT, Mostaghimi P, Da Wang Y, Liu S, Zhao C, Regenauer-Lieb K, Tung PKM. Deep learning for full-feature x-ray microcomputed tomography segmentation of proton electron membrane fuel cells. Comput Chem Eng 2022;161:107768.
[6] Cárdenas B, Swinfen-Styles L, Rouse J, Hoskin A, Xu W, Garvey S. Energy storage capacity vs. renewable penetration: a study for the UK. Renew Energy 2021;171:849–67.
[7] Wallace RL, Cai Z, Zhang H, Zhang K, Guo C. Utility-scale subsurface hydrogen storage: UK perspectives and technology. Int J Hydrogen Energy 2021;46(49):25137–59.
[8] Hashemi L, Blunt M, Hajibeygi H. Pore-scale modelling and sensitivity analyses of hydrogen-brine multiphase flow in geological porous media. Sci Rep 2021;11:8348. https://doi.org/10.1038/s41598-021-87490-7.
[9] Deane JP, Gallachóir BÓ, McKeogh E. Techno-economic review of existing and new pumped hydro energy storage plant. Renew Sustain Energy Rev 2010;14(4):1293–302.
[10] Katz DL, Tek MR. Overview on underground storage of natural gas. J Petrol Technol 1981;33:943–51. 06.
[11] Tarkowski R. Underground hydrogen storage: characteristics and prospects. Renew Sustain Energy Rev 2019;105:86–94.
[12] Aftab A, Hassanpouryouzband A, Xie Q, Machuca LL, Sarmadivaleh M. Toward a fundamental understanding of geological hydrogen storage. Ind Eng Chem Res 2022;61(9):3233–53.
[13] Hassanpouryouzband A, Joonaki E, Edlmann K, Haszeldine RS. Offshore geological storage of hydrogen: is this our best option to achieve net-zero? ACS Energy Lett 2021;6(6):2181–6.
[14] Tarkowski R, Uliasz-Misiak B. Towards underground hydrogen storage: a review of barriers. Renew Sustain Energy Rev 2022;162:112451.
[15] Okoroafor ER, Saltzer SD, Kovscek AR. Toward underground hydrogen storage in porous media: Reservoir engineering insights. Int J Hydrogen Energy 2022;47(79):33781–802.
[16] Feldmann F, Hagemann B, Ganzer L, Panfilov M. Numerical simulation of hydrodynamic and gas mixing processes in underground hydrogen storages. Environ Earth Sci 2016;75(16):1–15.
[17] Luboń K, Tarkowski R. Numerical simulation of hydrogen injection and withdrawal to and from a deep aquifer in nw Poland. Int J Hydrogen Energy 2020;45(3):2068–83.
[18] Pfeiffer WT, Beyer C, Bauer S. Hydrogen storage in a heterogeneous sandstone formation: dimensioning and induced hydraulic effects. Petrol Geosci 2017;23(3):315–26.
[19] Zamehrian M, Sedaee B. Underground hydrogen storage in a partially depleted gas condensate reservoir: influence of cushion gas. J Petrol Sci Eng 2022;212:110304.
[20] Lysyy M, Fernø M, Ersland G. Seasonal hydrogen storage in a depleted oil and gas field. Int J Hydrogen Energy 2021;46(49):25160–74.
[21] Salehi F, Abbassi R, Asadnia M, Chan B, Chen L. Overview of safety practices in sustainable hydrogen economy – An Australian perspective. Int J Hydrogen Energy 2022;47:34689–703.
[22] Yu M, Wang K, Vredenburg H. Insights into low-carbon hydrogen production methods: green, blue and aqua hydrogen. Int J Hydrogen Energy 2021;46(41):21261–73.
[23] Bo Z, Zeng L, Chen Y, Xie Q. Geochemical reactions-induced hydrogen loss during underground hydrogen storage in sandstone reservoirs. Int J Hydrogen Energy 2021;46(38):19998–20009.
[24] Sambo C, Dudun A, Samuel SA, Esenenjor P, Muhammed NS, Haq B. A review on worldwide underground hydrogen storage operating and potential fields. Int J Hydrogen Energy 2022;47:22840–80.
[25] Iglauer S, Ali M, Keshavarz A. Hydrogen wettability of sandstone reservoirs: implications for hydrogen geo-storage. Geophys Res Lett 2021;48(3):e2020GL090814.
[26] Hashemi L, Boon M, Glerum W, Farajzadeh R, Hajibeygi H. A comparative study for h2–ch4 mixture wettability in sandstone porous rocks relevant to underground hydrogen storage. Adv Water Resour 2022;163:104165.
[27] Lysyy M, Ersland G, Fernø M. Pore-scale dynamics for underground porous media hydrogen storage. Adv Water Resour 2022;163:104167.
[28] van Rooijen W, Hashemi L, Boon M, Farajzadeh R, Hajibeygi H. Microfluidics-based analysis of dynamic contact angles relevant for underground hydrogen storage. Adv Water Resour 2022:104221.
[29] Ni H, Boon M, Garing C, Benson SM. Predicting co2 residual trapping ability based on experimental petrophysical properties for different sandstone types. Int J Greenh Gas Control 2019;86:158–76.
[30] Oak M. Three-phase relative permeability of water-wet berea. 0–100. In: SPE/DOE enhanced oil recovery symposium. OnePetro; 1990.
[31] Alizadeh A, Piri M. Three-phase flow in porous media: a review of experimental studies on relative permeability. Rev Geophys 2014;52(3):468–521.
[32] Fatemi SM, Sohrabi M. Relative permeabilities hysteresis for oil/water, gas/water and gas/oil systems in mixed-wet rocks. J Petrol Sci Eng 2018;161:559–81.
[33] Krevor S, Blunt MJ, Benson SM, Pentland CH, Reynolds C, Al-Menhali A, Niu B. Capillary trapping for geologic carbon dioxide storage–from pore scale physics to field scale implications. Int J Greenh Gas Control 2015;40:221–37.
[34] Juanes R, Spiteri E, Orr Jr F, Blunt M. Impact of relative permeability hysteresis on geological co2 storage. Water Resour Res 2006;42(12).
[35] Akbarabadi M, Piri M. Relative permeability hysteresis and capillary trapping characteristics of supercritical co2/brine systems: an experimental study at reservoir conditions. Adv Water Resour 2013;52:190–206.
[36] Boon M, Hajibeygi H. Experimental characterization of H_2/water multiphase flow in heterogeneous sandstone rock at the core scale relevant for underground hydrogen storage (UHS). Scientific Reports 2022;12(1):1–12. https://doi.org/10.1038/s41598-022-18759-8.
[37] Lysyy M, Føyen T, Johannesen EB, Fernø M, Ersland G. Hydrogen relative permeability hysteresis in underground storage. Geophys Res Lett 2022:e2022GL100364.
[38] Energy S. A petrophysical model of the waarre formation in the Port Campbell embayment. In: Tech. Rep. Victorian gas program technical report 17. Geological Survey of Victoria; 2020.
[39] Mahdi DS, Al-Khdheeawi EA, Yuan Y, Zhang Y, Iglauer S. Hydrogen underground storage efficiency in a heterogeneous sandstone reservoir. Advances in Geo-Energy Research 2021;5(4):437.
[40] Wang G, Pickup G, Sorbie K, Mackay E. Scaling analysis of hydrogen flow with carbon dioxide cushion gas in subsurface heterogeneous porous media. Int J Hydrogen Energy 2022;47(3):1752–64.
[41] Kanaani M, Sedaee B, Asadian-Pakfar M. Role of cushion gas on underground hydrogen storage in depleted oil reservoirs. J Energy Storage 2022;45:103783.

[42] Krevor SC, Pini R, Zuo L, Benson SM. Relative permeability and trapping of co2 and water in sandstone rocks at reservoir conditions. Water Resour Res 2012;48(2).
[43] Pini R, Krevor SC, Benson SM. Capillary pressure and heterogeneity for the co2/water system in sandstone rocks at reservoir conditions. Adv Water Resour 2012;38:48–59.
[44] Yekta A, Manceau J-C, Gaboreau S, Pichavant M, Audigane P. Determination of hydrogen–water relative permeability and capillary pressure in sandstone: application to underground hydrogen injection in sedimentary formations. Transport Porous Media 2018;122(2):333–56.
[45] Oostrom M, White M, Porse S, Krevor S, Mathias S. Comparison of relative permeability–saturation–capillary pressure models for simulation of reservoir co2 injection. Int J Greenh Gas Control 2016;45:70–85.
[46] Lenhard RJ, Parker JC, Mishra S. On the correspondence between brooks-corey and van genuchten models. J Irrigat Drain Eng 1989;115(4):744–51. https://doi.org/10.1061/(ASCE)0733-9437(1989)115:4(744). publisher: American Society of Civil Engineers.
[47] Land CS. Calculation of imbibition relative permeability for two-and three-phase flow from rock properties. Soc Petrol Eng J 1968;8:149–56. 02.
[48] Killough J. Reservoir simulation with history-dependent saturation functions. Soc Petrol Eng J 1976;16:37–48. 01.
[49] Ershadnia R, Hajirezaie S, Amooie A, Wallace CD, Gershenzon NI, Hosseini SA, Sturmer DM, Ritzi RW, Soltanian MR. Co2 geological sequestration in multiscale heterogeneous aquifers: effects of heterogeneity, connectivity, impurity, and hysteresis. Adv Water Resour 2021;151:103895.
[50] Niu B, Al-Menhali A, Krevor SC. The impact of reservoir conditions on the residual trapping of carbon dioxide in b erea sandstone. Water Resour Res 2015;51(4):2009–29.
[51] Aziz K. Petroleum reservoir simulation, vol. 476. Applied Science Publishers; 1979.
[52] C. M. Group. User's guide GEM, advanced compositional reservoir simulator (version 2020). Computer Modeling Group Ltd, Calgary., Computer Modeling Group; 2020. URL, https://www.cmgl.ca/gem.
[53] Energy S. Dynamic modelling of the Fenton Creek gas field. In: Tech. Rep. Victorian gas program technical report 43. Geological Survey of Victoria; 2020.
[54] Delshad M, Umurzakov Y, Sepehrnoori K, Eichhubl P, Batista Fernandes BR. Hydrogen storage assessment in depleted oil reservoir and saline aquifer. Energies 2022;15(21):8132.
[55] Robinson DB, Peng D-Y. The characterization of the heptanes and heavier fractions for the GPA Peng-Robinson programs. Gas processors association; 1978.
[56] Chuang S-Y, Chappelear PS, Kobayashi R. Viscosity of methane, hydrogen, and four mixtures of methane and hydrogen from-100. degree. c to 0. degree. c at high pressures. J Chem Eng Data 1976;21(4):403–11.
[57] Hernandez-Gomez R, Tuma D, Perez E, Chamorro CR. Accurate experimental (p, ρ, and t) data for the introduction of hydrogen into the natural gas grid (ii): thermodynamic characterization of the methane–hydrogen binary system from 240 to 350 k and pressures up to 20 mpa. J Chem Eng Data 2018;63(5):1613–30.
[58] Flesch S, Pudlo D, Albrecht D, Jacob A, Enzmann F. Hydrogen underground storage—petrographic and petrophysical variations in reservoir sandstones from laboratory experiments under simulated reservoir conditions. Int J Hydrogen Energy 2018;43(45):20822–35.
[59] Ramesh Kumar K, Makhmutov A, Spiers CJ, Hajibeygi H. Geomechanical simulation of energy storage in salt formations. Sci Rep 2021;11:19640. https://doi.org/10.1038/s41598-021-99161-8.
[60] Ramesh Kumar K, Hajibeygi H. Multiscale simulation of inelastic creep deformation for geological rocks. J Comput Phys 2021;440:110439. https://doi.org/10.1016/j.jcp.2021.110439.
[61] Delshad M, Alhotan M, Batista Fernandes BR, Umurzakov Y, Sepehrnoori K. Pros and cons of saline aquifers against depleted hydrocarbon reservoirs for hydrogen energy storage. In: SPE annual technical conference and exhibition. OnePetro; 2022. SPE–210351–MS.